ARTICLE NO. 80-4112

Slag and Other Liquid Behavior on Vertical Surface at Near-Freezing Temperature

Kwan H. Im*
Argonne National Laboratory, Argonne, Ill.
and
Paul M. Chung†
University of Illinois at Chicago Circle, Chicago, Ill.

Deposition of liquid droplets from turbulent stream to vertical surface and the subsequent transient behavior of the liquid layer are analyzed for the surface temperatures near the freezing point of the liquid. General wave behavior of the equations governing the liquid layer is elucidated. The analysis is applied to the problem of slag layer accumulation on the passage walls of a magnetohydrodynamic regenerative heat exchanger using the coal combustion product as the heat source. The wave behavior predicts the emergence of an accumulation shock that leads to clogging of the passages for certain cyclic operations.

Nomenclature

a_i = droplet radius
C = mass fraction
C_i = mass fraction of the ith size group droplets
C_{io} = average mass fraction of the ith size group droplets in the core region
D = molecular diffusivity
f_i = function defined by Eq. (43)
g = gravitational constant
h = heat-transfer coefficient based on $T_{gs} - T_{ga}$
h_m = mass-transfer coefficient based on $C_{gs} - C_{ga}$
Δh^0 = heat of condensation
I = enthalpy defined by Eq. (27)
k = molecular conductivity
L = length of the vertical surface
ℓ = mixing length
M = function defined by Eq. (17)
Nu = Nusselt number defined by Eq. (22)
Pr = Prandtl number
q = heat flux in the direction of $-y$
R = pipe radius
Re = Reynolds number based on 2R
s = characteristic direction defined by Eqs. (17) and (19)
Sc = Schmidt number
Sh = Sherwood number defined by Eqs. (22)
S_i = overshooting distance of the ith size group particles
T = absolute temperature
t = time
U = nondimensional velocity defined in Eq. (11)
u = x component of velocity
u_{go} = average gas velocity in the core region
u^+ = u/v^*
V_i = overshooting velocity of the ith size group droplets
v^* = friction velocity of the gas phase
W = condensation flux at the liquid gas interface
X = x/L
x = streamwise coordinate
Y = y/δ
y = coordinate normal to the surface
y^+ = yv^*/ν_g
α = thermal diffusivity
β = mean surface roughness scale
Δ = δ/δ_0
δ = liquid layer thickness
ϵ_i = turbulent diffusivity of the ith size group droplets
θ = T/T_0
μ = dynamic viscosity (of liquid with no subscript)
$\hat{\mu}$ = normalized liquid viscosity, μ/μ_0
ν = kinematic viscosity (of liquid with no subscript)
ρ = density (of liquid with no subscript)
τ = t/t_0
τ_s = shear stress at the gas-liquid interface
ω_p = particle frequency
ω_t = turbulence frequency

Subscripts

a = average over the pipe cross section
b = edge of the buffer layer
g = gas phase
L = liquid phase
o = reference quantities defined by Eqs. (10)
s = gas-liquid interface
w = pipe wall
∞ = inlet to pipe

Received Sept. 7, 1979; revision received April 25, 1980. This paper is declared a work of the U.S. Government and therefore is in the public domain.

Index categories: Ablation, Pyrolysis, Thermal Decomposition and Degradation (including Refractories); MHD; Boundary Layers and Convective Heat Transfer—Turbulent.

*Mechanical Engineer, Engineering Division. Member AIAA.
†Dean of Engineering. Member AIAA.

I. Introduction

OFTEN in nature and industrial machines, condensation and flow take place near the freezing temperature of the liquid. Formation of outdoor icicles and emergence of ice bulges on certain refrigerated surfaces are common phenomena caused by the process of condensation and flow.

The present study of this process is motivated by the need for a better understanding of the influence of the slag (molten ash) and molten seed (potassium salt) on the performance of the heat exchangers in the coal-fired MHD powerplants.[1-3] Air preheaters for the coal combustors are designed as vertical regenerative heat exchangers with the combustion product as the heat source. During the regenerative period, the combustion product containing the slag and seed droplets, as well as their vapors, flow through the heat exchanger passages which are usually vertical cylindrical openings. During the blowdown period, the slag layers and exchanger walls are cooled by the air. At the completion of this period and at the

beginning of the regeneration, portions of the walls are at or below the freezing point of the slag. Depending on the amplitudes and periods of the regenerative and blowdown cycles and other operating parameters, excessive localized slag accumulation could take place and seriously impair performance of the heat exchanger.

In the present study, a basic and general understanding of the transient behavior of the condensate near freezing temperature under the influence of the gravity is sought rather than specific information on the slagging MHD heat exchangers. General behavior of the freezing liquid layer on a semi-infinite vertical plate is studied; criteria for emergence of the localized bulge (accumulation shock) are elucidated in Sec. II. Turbulent transport of the droplets to the liquid layer is analyzed in Sec. III, and in Sec. IV, the results of Secs. II and III are combined to describe the emergence of accumulation shock in a typical slagging MHD regenerative heat exchanger.

II. Liquid Layer

Formulation

We consider a semi-infinite vertical plate in contact with a turbulent gas stream containing liquid droplets and their vapor as shown in Fig. 1. The wall temperature is considered to be a given function of time and location. The gas temperature and mass fractions C_i are specified at $x=0$, and their distributions in x are governed by the conservation equations to be discussed later.

The wall temperatures are specified to be below condensation temperature of the vapor at all times, and furthermore, portions of the wall temperature are specified to be below the freezing point, at least for a certain period of time.

Equations governing the liquid layer are as follows.

Continuity:

$$\frac{\partial \delta(x,t)}{\partial t} + \frac{\partial}{\partial x}\int_0^{\delta(x,t)} u\,dy = \frac{W}{\rho} \tag{1}$$

Momentum:

$$\frac{\partial}{\partial y}\left(\mu \frac{\partial u}{\partial y}\right) = -\rho g \tag{2}$$

Energy:

$$k\frac{\partial T}{\partial y} = q \tag{3}$$

It is assumed in the momentum equation that the fluid behavior is Newtonian all the way down to the freezing point.

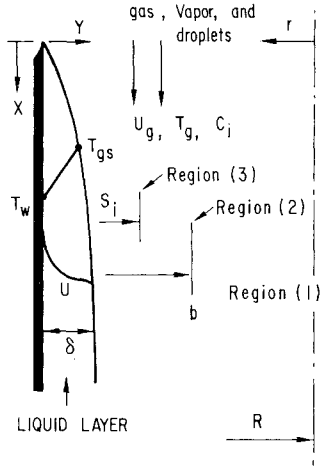

Fig. 1 Condensation on a vertical plate or interior tube wall: region 1 = turbulent core, region 2 = buffer layer, region 3 = overshooting region.

Such approximation should be acceptable as it was with the melting ablation problems studied earlier.[4,5]

Since the Reynolds number is expected to be small in the liquid layer, the convection terms are neglected in Eqs. (2) and (3). It is also anticipated that the characteristic transient time of the imposed wall temperature will be much longer than the characteristic momentum and energy response times of the liquid layer δ^2/ν and $\delta^2/(k/\rho c_p)$. Therefore, quasi-steady approximation is made in Eqs. (2) and (3).

The initial and boundary conditions are specified as follows:

Initial:

$$\delta = 0, \text{ for all } x \tag{4}$$

Boundary:

At $x=0$,

$$\delta = 0, \text{ for all } t \tag{5}$$

At $y=0$,

$$u = 0 \tag{6}$$

$$T = T_w(x,t) \tag{7}$$

At $y=\delta$,

$$\mu\frac{\partial u}{\partial y} = \tau_s \tag{8}$$

$$k\frac{\partial T}{\partial y} = k_g\frac{\partial T_g}{\partial y} = q_s \tag{9}$$

Remembering the fact that q is an unknown function, Eqs. (1-3) require six initial and boundary conditions. Equations (4-9) comprise the required six.

In Eq. (1), W denotes the liquid mass deposition flux at the layer surface. This function is determined from the analysis of the gas stream to be discussed in a subsequent section.

Liquid Layer Equation

The purpose of the remainder of this section is to elucidate the general behavior of the liquid layer. This can be accomplished more effectively by neglecting τ_s; it will, however, be reinstated in the subsequent numerical solutions.

First, a set of appropriate reference quantities is chosen as follows. The characteristic velocity, liquid-layer response time, and layer thickness must be dictated by the kinematic viscosity of the fluid and the gravity which causes the flow. These reference quantities are, therefore, chosen as:

$$u_0 = (\nu_0 g)^{1/3} \tag{10a}$$

$$t_0 = L/(g\nu_0)^{1/3} \tag{10b}$$

$$\delta_0 = (\nu_0^2/g)^{1/3} \tag{10c}$$

The length along the plate is a given reference quantity. Therefore, the characteristic length of the plate is specified as L. Using these reference quantities, a set of dimensionless variables is defined as:

$$U = u/u_0 = u/(\nu_0 g)^{1/3} \tag{11}$$

$$\tau = t/t_0 = t(g\nu_0)^{1/3}/L \tag{12}$$

$$\Delta = \delta/\delta_0 = \delta(g/\nu_0^2)^{1/3} \tag{13}$$

and

$$X = x/L$$

Having defined appropriate dimensionless quantities, we proceed with the analysis as follows. Equation (2) is first

integrated to satisfy Eqs. (6) and (8). The result is then substituted into Eq. (1) for u. This equation becomes, in terms of the dimensionless quantities, Eqs. (11-13),

$$\frac{\partial \Delta}{\partial \tau} + \frac{\partial}{\partial X}\left(\frac{\Delta^3}{\hat{\mu}_w} M\right) = \frac{L}{\nu_0}\frac{W}{\rho} \tag{14}$$

where

$$\hat{\mu}_w = \mu_w/\mu_0 \tag{15}$$

and

$$M = \int_0^1 \frac{(1-Y)^2}{(\mu/\mu_w)}\,dY \tag{16}$$

The remaining equation, Eq. (3), is not needed for the immediate general discussion.

General Behavior

Equation (14) is a wave equation and its behavior can be understood best on a wave plane. The characteristic direction of Eq. (14) is given by

$$\frac{d\tau}{dX} = \frac{\hat{\mu}_w}{3M\Delta^2} \tag{17}$$

Along the characteristics, Eq. (14) is transformed into the compatibility relationship

$$\frac{d\Delta}{ds} = \left[\frac{\Delta^3}{\hat{\mu}_w^2}\left(M\frac{d\hat{\mu}_w}{dX} - \hat{\mu}_w\frac{dM}{dX}\right) + \frac{L}{\nu_0}\frac{W}{\rho}\right]\left[1+\left(\frac{3M\Delta^2}{\hat{\mu}_w}\right)^2\right]^{-1/2} \tag{18}$$

where

$$ds = (dX^2 + d\tau^2)^{1/2} \tag{19}$$

With the viscosity normalized by its wall value, M, as defined by Eq. (16), will be a rather weak function of X. Therefore, for a given deposition rate W, Eqs. (17) and (18) show that the structure of the layer is largely governed by the viscosity variation along the wall $\hat{\mu}_w$. With this in mind, let us study the qualitative behavior of Eqs. (17) and (18) with the aid of the wave diagram, Fig. 2.

Figure 2 qualitatively delineates evolution of the liquid layer until the incipient formation of the accumulation shock, based on Eqs. (17) and (18). In this description, the wall temperature is considered to decrease in the direction of X passing through a freezing point of the fluid somewhere downstream. It is also considered that the wall temperature is continuously cycled with equal heating and cooling periods.

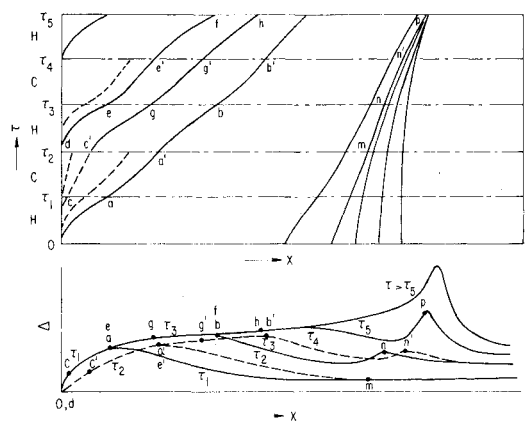

Fig. 2 Qualitative wave diagram for liquid layer.

In Fig. 2, H and C denote the heating and cooling periods, respectively. The deposition rate W is considered to decrease in the direction of X during the heating period, whereas it is zero for all X during the cooling portion of the cycle.

Typical characteristics are shown on the τ-X plane, whereas the corresponding layer profiles are sketched on the Δ-X plane.

At $\tau=0$, $\Delta=0$ for all X. At the end of the first heating period, Δ profile is that which is labeled $\tau=\tau_1$. This profile is mainly dictated by the W term in Eq. (18). Equation (17) shows that $d\tau/dX\to\infty$ at $\tau=0$ where $\Delta=0$. For $\tau>0$, $\Delta>0$ and $d\tau/dX$ becomes finite for $X>0$. For $X<0$, on the other hand, $d\tau/dX=\infty$ for all τ. Therefore, a characteristic "fan" emanates from the $X=\tau=0$ point filling the space between the first characteristic $\overline{oa}$, and the last characteristic which is the τ axis. The fan is shown by the broken lines.

During the cooling period, $W=0$. As mentioned earlier, M probably is a weak function of X, and dM/dX may be small in Eq. (18). $d\hat{\mu}_w/dX>0$ and it may become very large near the freezing point. The quantity $(d\hat{\mu}_w/dX)/\hat{\mu}_w^2$, however, may be rather small since $\hat{\mu}_w^2$ increases rapidly with the decreasing wall temperature. Therefore, Δ varies little along a characteristic during the cooling period, according to Eq. (18). Hence, $\Delta_{a'}\simeq\Delta_a, \Delta_{c'}\simeq\Delta_c$, etc., and this engenders the Δ profile for $\tau=\tau_2$ shown in Fig. 2.

As mentioned previously, $W(>0)$ is the predominant term on the right-hand side of Eq. (18) during the heating period, and Δ increases along the characteristics resulting in the Δ profile for $\tau=\tau_3$ shown. The first characteristic $\overline{de}$ is identical to the first characteristic $\overline{oa}$. Also, the characteristic fan filling the span between $\overline{de}$ and the τ axis is identical to that between $\overline{oa}$ and the τ axis. Therefore, the Δ profile between o and e obtained at the end of the second heating period, τ_3, is the same as that between o and a obtained at the end of the first heating period, τ_1.

Since the characteristic $\overline{de}$ is identical to the characteristic $\overline{oa}$, their continuations, $\overline{ee'}$ and $\overline{aa'}$, respectively, are also identical. Furthermore, all other characteristics filling the space between the τ axis and $\overline{ee'}$ are the same as those between the τ axis and $\overline{aa'}$. This is true because these two groups of characteristics are the continuations of the fans generated during the second and first heating periods, respectively, and these two fans are identical, as previously stated. Therefore, the Δ profile between o and e' obtained at the end of the second cooling period, τ_4, is identical to that between o and a' obtained at the end of the first cooling period, τ_2.

It is now clear that a steady-state Δ profile is attained up to X_a, X_b, etc. at the ends of the heating periods, τ_1, τ_3, etc., respectively, and that another steady-state Δ profile emerges up to $X_{a'}$, $X_{b'}$, etc. at the ends of the cooling periods τ_2, τ_4, etc., respectively. Therefore, on that portion of the plate traversed by the first characteristic emanating from the leading edge ($oaa'bb'$----), the liquid layer will oscillate between the two steady-state profiles ad infinitum.

Accumulation Shock

Returning to Eqs. (17) and (18), the only significant term on the right-hand side of Eq. (18) is W, as was stated earlier. Since W varies slowly with respect to X during the heating period, and is zero during the cooling period, Eq. (18) is expected to behave rather well. On the other hand, Eq. (17) shows that $d\tau/dX$ increases with $\hat{\mu}_w$ and, therefore, the characteristics will coalesce as $\hat{\mu}_w$ increases along X with the decreasing wall temperature. As the freezing point is traversed, $\hat{\mu}_w$ and, therefore, $d\tau/dX$, will approach infinity. Before that point, however, coalescing of the characteristics will engender an accumulation "shock," which is defined as the rapid localized increase of the liquid layer thickness—precipitous emergence of a liquid layer bulge. The time and position of the shock emergence are largely dictated by the manner of coalescence of the characteristics. It is clear from Eq. (17), however, that the coalescence is more likely to take

place where $d\hat{\mu}_w/dX$ is large, such that the succeeding characteristics have greater slopes than the preceding ones (see Fig. 2).

Having discussed the expected general behavior of the liquid layer, the deposition rate W will be quantified in the next section for a specific application. Numerical solution of the governing equations will then ensue.

III. Gas Phase with Particulate Matters

With subsequent application to the coal-fired regenerative heat exchanger in mind, turbulent pipe flow of the gas-liquid droplet mixture is considered. In such systems, concentration of the droplets is sufficiently small so that the droplets have a negligible influence on the flow and energy of the gas phase. Transport of the energy and condensible gaseous species (vapor) are then decoupled from that of the droplets and can be described readily in terms of the existing solutions. On the other hand, transport of the droplets is rather complicated for a turbulent stream. These transport processes are discussed in the following.

Energy and Vapor

With the flow and energy considered to be decoupled from the droplet behavior, the following simple energy equation is constructed in terms of the Nusselt number well known for turbulent pipe flow.

$$u_{ga}R\frac{dT_{ga}}{dx}=Nu\frac{\alpha_g}{R}(T_{gs}-T_{ga}) \tag{20}$$

Similarly, a conservation equation for the vapor is written in terms of the corresponding Sherwood number as

$$u_{ga}R\frac{dC_{ga}}{dx}=Sh\frac{D_g}{R}(C_{gs}-C_{ga}) \tag{21}$$

In the above equations, Nu and Sh are given by[6,7]

$$Nu=2Rh/k=0.023Re^{0.8}Pr_g^{1/3} \tag{22a}$$

and

$$Sh=2Rh_m/\rho_g D_g=0.023Re^{0.8}Sc_g^{1/3} \tag{22b}$$

Boundary conditions for Eqs. (20) and (21) are:

At $x=0$,

$$T_{ga}=T_{ga\infty},\quad C_{ga}=C_{ga\infty} \tag{23}$$

and at $y=0$ (at s),

$$q_{sg}=q_{sL}=q_s,\quad T_{gs}=T_s \tag{24}$$

and

$$C_{gs}=C_{gs}(T_{gs}) \tag{25}$$

Each of Eqs. (20) and (21) requires one boundary condition with respect to x, and specification of the variable at the interface s. Since the interface temperature T_{gs} $(=T_s)$ is not known a priori, the additional condition, $q_{sg}=q_{sL}$, is required.

When $D_g=\alpha_g$, Nusselt and Sherwood numbers are equal, and the interface heat transfer can be written as

$$q_{sg}=\frac{\mu_g}{Pr_g}\frac{Nu}{2R}(I_{ga}-I_{gs}) \tag{26}$$

where

$$I_g=c_{pg}T_g+\Delta h^0 C_g \tag{27}$$

The condensation rate is given by

$$W_{gs}=\frac{\mu_g}{Sc_g}\frac{Sh}{2R}(C_{ga}-C_{gs}) \tag{28}$$

Solutions of Eqs. (20) and (21) are obtained numerically.

Droplets (Particulate Matter)

Deposition of droplets or solid particles on surfaces is caused by three different mechanisms, depending on the particle size. The submicron size particles are transported to the laminar sublayer by the fluid turbulence in essentially the same manner as the turbulent transport of gaseous species. Diffusion through the sublayer is then accomplished by the thermal force (thermophoresis) generated by the steep temperature gradient. The thermophoresis particle transport was analyzed previously.[8] Particles between about 1 and 60 μm in size are transported to within the "overshooting" distance from the surface by the fluid turbulence. However, different from the turbulent transport of the submicron size particles, these particles do not necessarily follow the fluid turbulence. Especially, the particles continue their motion toward the surface and are deposited because of the momentum imparted to them by the turbulent eddies at the overshooting distance. Finally, the particles greater than about 60 μm in size are little influenced by fluid turbulence and impinge on surfaces that cross their mean trajectories.

As was mentioned, the thermophoretic transport was studied previously.[8] In the present paper, the second mechanism will be analyzed. Particles of size between 1 and 100 μm are most prevalent in the scale model experiments[9,10] of the coal-fired regenerative heat exchanger.

Assuming that the particles can be categorized into a finite number of different size groups, a conservation equation of the ith size particles is constructed as

$$u_g\frac{\partial C_i}{\partial x}=\frac{1}{(R-y)}\frac{\partial}{\partial y}\left[(R-y)\epsilon_i\frac{\partial C_i}{\partial y}\right] \tag{29}$$

Figure 1 shows the coordinate system. Boundary conditions of Eq. (29) are:

At $x=0$,

$$C_i=C_{i\infty} \tag{30}$$

At $y=R$,

$$\frac{\partial C_i}{\partial y}=0 \tag{31}$$

At $y=S_i$,

$$\epsilon_i\frac{\partial C_i}{\partial y}=V_i C_{is} \tag{32}$$

where S_i and V_i are the particle overshooting distance and velocity, respectively, and are given by[11,12]

$$S_i=(V_i/\omega_{pi})+a_i+\beta \tag{33a}$$

and

$$V_i=v^*/[1+(\omega_t/\omega_{pi})]^{1/2} \tag{33b}$$

The turbulence and particle response frequencies, ω_t and ω_{pi}, are approximated by

$$\omega_t=v^*/\ell \tag{34a}$$

and

$$\omega_{pi}=9\mu_g/(2\rho a_i^2) \tag{34b}$$

The problem at hand is to solve Eq. (29) for all $x>0$ and $S_i \leq y \leq R$, and to satisfy the boundary conditions, Eqs. (30-32). In order to facilitate the solution, we assume first that the liquid layer thickness is negligible compared to the pipe radius and then we divide the flowfield into the following three regions (see Fig. 1): 1) turbulent core region $b \leqq y \leqq R$; 2) turbulent diffusion region (buffer layer) $S_i \leqq y \leqq b$; and 3) overshooting region $0 \leqq y \leqq S_i$.

In region 1, the radial mixing is considered to be complete so that u_g and C_i are uniform with respect to r. In region 2, turbulent transport of the particles takes place with the diffusivity[11,12]

$$\epsilon_i = \epsilon_g / [1 + (\omega_t / \omega_{pi})] \tag{35}$$

The gas eddy diffusivity ϵ_g is given by[6,7]

$$\epsilon_g = 0.0154 \nu_g u^+ y^+ [1 - \exp(-0.0154 u^+ y^+)] \tag{36}$$

where

$$\begin{aligned} u^+ &= y^+ && \text{for } y^+ < 5 \\ u^+ &= -3.05 + 5.0 \ln y^+ && \text{for } 5 \leqq y^+ \leqq 30 \\ u^+ &= 5.5 + 2.5 \ln y^+ && \text{for } y^+ > 30 \end{aligned} \tag{37}$$

Equations (35-37) are valid outside of the laminar sublayer. However, the thickness of the overshooting region is greater than that of the laminar sublayer for the particle sizes of interest presently. Therefore, these equations are sufficient for the buffer layer study.

As seen in Eqs. (33), the overshooting distance S_i is a function of the particle size, and it defines the distance through which the turbulent eddies are able to propel the particles. Therefore, the mass flux of the propelled ith size particles at S_i given by Eq. (32) remains constant through region 3, and it represents the mass deposition flux at the surface. Solution of Eq. (29) now proceeds as follows.

Integration of Eq. (29) with respect to y between b and R for region 1 gives

$$\frac{u_{go}(R-b)}{2} \frac{dC_{io}}{dx} = -\left(\epsilon_i \frac{\partial C_i}{\partial y}\right)_b \tag{38}$$

where the boundary condition, Eq. (31), has been applied. Next, integration of Eq. (29) across region 2 results in

$$\frac{d}{dx} \int_{S_i}^{b} u_g(y) C_i(x,y)\, dy = \left(\epsilon_i \frac{\partial C_i}{\partial y}\right)_b - \left(\epsilon_i \frac{\partial C_i}{\partial y}\right)_{S_i} \tag{39}$$

In deriving the above equations, the overshooting distance was assumed to be negligibly small compared to the pipe radius. Substituting Eq. (38) for the first term on the right-hand side of Eq. (39), and applying the boundary condition, Eq. (32), we obtain

$$u_{go} \frac{(R-b)}{2} \frac{dC_{io}}{dx} + \frac{d}{dx} \int_{S_i}^{b} u_g(y) C_i(x,y)\, dy = V_i C_{i_{S_i}} \tag{40}$$

We now seek the solution of this equation satisfying the remaining boundary condition, Eq. (30). After Pohlhausen,[6] we shall first assume a suitable profile for C_i in the integrand of the integrodifferential Eq. (40) and reduce it to a differential equation. The profile is constructed from the first-order solution of the original equation, Eq. (29), as follows. We neglect the convection term, $u_g \partial C_i / \partial x$, for the buffer layer and integrate Eq. (29) with respect to y. Then as we apply the boundary condition, Eq. (32), and condition $C_i(x,b) = C_{io}(x)$, there results the first-order C_i profile,

$$C_i(x,y) = C_{io}(x) \left[1 + V_i \int_{S_i}^{y} \frac{dz}{\epsilon_i(z)}\right] \Big/ \left[1 + V_i \int_{S_i}^{b} \frac{dz}{\epsilon_i(z)}\right] \tag{41}$$

Returning to Eq. (40), we substitute the above profile for $C_i(x,y)$ and integrate the resulting equation with respect to x. After satisfying the boundary condition, Eq. (30), we obtain the solution for $C_{io}(x)$:

$$C_{io}(x) = C_{i\infty} \exp(-f_i x) \tag{42}$$

where

$$f_i = \left[\frac{V_i}{1 + V_i \int_{S_i}^{b} \frac{dz}{\epsilon_i(z)}}\right] \Bigg/ \left\{\frac{(R-b)u_{go}}{2} + \frac{V_i \int_{S_i}^{b} dy\, u_g(y) \left[1 + V_i \int_{S_i}^{y} \frac{dz}{\epsilon_i(z)}\right]}{1 + V_i \int_{S_i}^{b} \frac{dz}{\epsilon_i(z)}}\right\} \tag{43}$$

Equation (41) then gives the C_i profile for region 2. Equations (41-43) constitute the formal solution of Eq. (40). The total deposition flux of the particles is obtained as

$$W_s = \sum_i W_{is} = \sum_i V_i C_i(x, S_i) \tag{44}$$

IV. Slag Layer on Heat Exchanger Walls

Problem Statement

Analysis of the solidifying liquid layer and the deposition rate given in the two preceding sections are employed herein to study the accumulation of the slag layer in the coal-fired heat exchangers. In an MHD open-cycle system,[1-3] the coal combustion product often is used as the regenerative heat source for the air preheaters. These preheaters basically consist of ceramic bricks with aligned vertical holes whose diameters are of the order of ¾ in.[9] They are designed to operate continuously with consecutive heating and cooling (blow-down) cycles. The ash vapor and the slag (molten ash) droplets contained in the combustion product deposit on the walls of the heater passages during the heating cycle. During the cooling cycle, the temperature of the lower portion of the heater walls is often depressed to below the freezing point of the slag. It is the main purpose of the present study to investigate the operating condition under which the "accumulation shock" may result. Such a shock will stymie continued operation of the heat exchanger in practice.

The gas phase analysis of the preceding section for pipe flow is directly applicable to that for the heat exchanger passages. The liquid layer analysis over the vertical plate of Sec. II is approximately valid for that on the heat exchanger walls.

It may be appropriate to point out here that for the actual MHD preheaters, the slag droplets would predominantly be submicron in size.[8] On the other hand, in the scale model experimental heat exchangers,[9,10] the droplet sizes are between 1 and 100 μm. In the present paper, the gas phase is considered to contain mostly droplets greater than 1 μm in size, and the analysis of Sec. III is employed. The deposition model based on the thermophoresis previously formulated[8] may be readily substituted for the analysis of Sec. III in the future study of the actual preheaters with the submicron size particles. In any case, as was stated in Sec. II, the basic

behavior of the liquid layer is quite immune to the mechanism of mass transfer, and, therefore, the numerical results to be obtained should have a general validity.

As discussed in Sec. II, variation of the liquid viscosity with respect to temperature is most important in describing the liquid layer behavior and possible formation of the shock. For the purpose of the present numerical example, we consider that the slag viscosity in poise is given by

$$\log_{10}\mu = 10^{7}\frac{B}{(T-423)} + C \tag{45}$$

for temperatures above the freezing temperature T_F where T is in degrees Kelvin. For $T \leqq T_F$, μ is assumed to be infinitely large. Constants B and C, and the freezing temperature are functions of composition of the slag. For a typical slag composition,[13,14] we take

$$B = 0.01043\,SiO_2 + 0.01003\,Al_2O_3 - 0.29629$$

$$C = -0.01542\,SiO_2 - 0.03881\,Al_2O_3 - 0.01617\,Fe_2O_3 - 0.00891\,CaO - 0.01293\,MgO + 1.04678$$

$$T_F = 3263 - 1470\hat{\alpha} + 360\,\hat{\alpha}^2 - 14.7\hat{\beta}^2 \tag{46a}$$

where

$$\hat{\alpha} = SiO_2/Al_2O_3$$

$$\hat{\beta} = Fe_2O_3 + CaO + MgO \tag{46b}$$

In the above expressions, SiO_2, Al_2O_3, etc., are mass fractions in percent such that

$$SiO_2 + Al_2O_3 + Fe_2O_3 + CaO + MgO = 100 \tag{46c}$$

It is noted that the slag viscosity and freezing temperature are not well established, and no claim is made herein on the accuracies of Eqs. (45) and (46).

We consider that a constant mass rate of the combustion gas flows through the vertical passage from top to bottom during the heating cycle. An equal rate of air flows through the passage in the opposite direction during the cooling cycle. The combustion gas contains liquid droplets with the following size distribution as shown in Table 1. Temperature of the heat passage wall is considered to vary with respect to x and time according to the following expression.

$$T_w(x,t) = (1750 - 129x) + (112 + 30x)\cos(\pi t/60) \tag{47}$$

where t is in minutes, T_w is in degrees Kelvin, and x in meters.

For the given mass flow rates and $T_w(x,t)$, variation of the liquid layer thickness with respect to x and t is sought.

Numerical Solutions

For the numerical solutions, it is assumed that the mass fraction of the slag in vapor phase is negligibly small as compared to that in the droplet form. The following coupled set of equations is solved numerically:

Liquid Layer: Eqs. (1-3) with the boundary conditions, Eqs. (4-9). The standard wall stress for turbulent pipe flow is employed for τ_s in Eq. (8).

Gas Phase: Eq. (20) with the boundary conditions, Eqs. (23) and (24). Equations (41-44) with the auxiliary equations (33-37). Note that the main coupling between the gas phase and liquid layer arises through Eqs. (24) and (44).

Numerical Technique: Besides the algebraic expressions, the governing equations include the ordinary differential, Eq. (20) and the partial differential, Eq. (1). The standard Runge-Kutta and finite-difference schemes were found to be readily applicable to the ordinary and partial-differential equations, respectively.

Table 1 Size distribution of droplets

Size range, μm	Mass fraction
7.5-12.5	0.05
12.5-22.5	0.10
22.5-37.5	0.20
37.5-52.5	0.25
52.5-67.5	0.20
67.5-82.5	0.15
82.5-97.5	0.05

Discussion of Numerical Results

Results of the computations are shown in Figs. 3-6. Equal heating and cooling cycle periods of 60 min are imposed on the problem.

Figure 3 shows the thickness profiles of the liquid layer at the ends of the three time periods. Incipient formation of the accumulation shock is evident after approximately 3000 min of heat exchanger operation at about 4 m from the top. At the end of about 5000 min, approximately one half of the passage cross sections will be plugged. This probably will result in an excess pressure drop through the heat exchanger and impair the continued operation.

The physical reason for and manner in which the shock emerges have been described in detail in Sec. II with the aid of the wave diagram, Fig. 2. For the particular set of operating conditions, the waves travel along the liquid layer establishing a steady-state behind up to $x \simeq 3.5$ m. The characteristics then coalesce resulting in the shock as discussed previously.

Figure 4 shows the layer profiles for the same operating conditions as Fig. 3, except that the gas flow rate is an order of magnitude greater. First, the shock begins to form much earlier than for the previous case because of the greater slag deposition rate. Location of the shock then gradually moves downward with the continued accumulation. At the end of

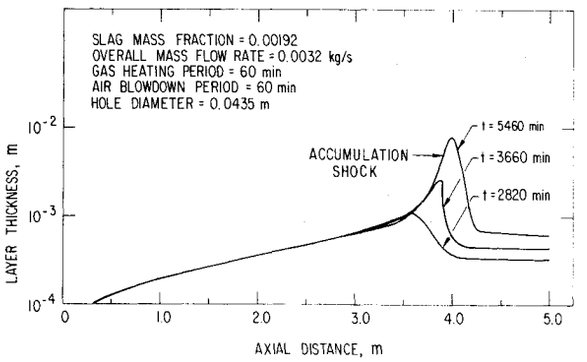

Fig. 3 Evolution of liquid layer profile for mass flow rate of 0.0032 kg/s.

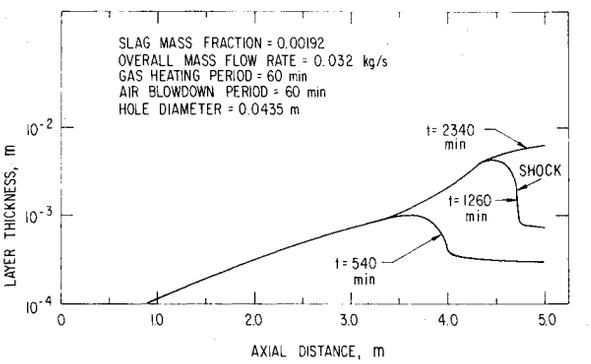

Fig. 4 Evolution of liquid layer profile for mass flow rate of 0.032 kg/s.

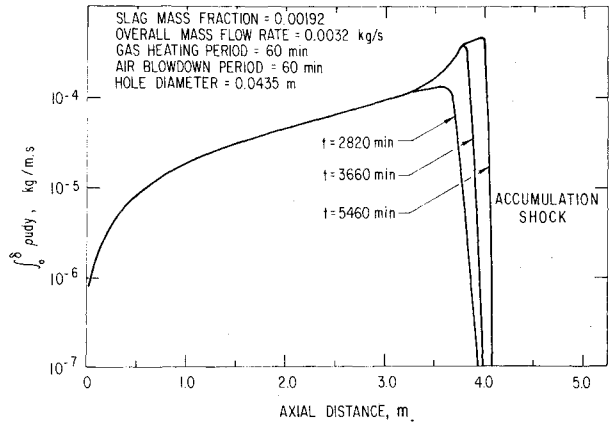

Fig. 5 Slag flow rate in liquid layer for mass flow rate of 0.0032 kg/s.

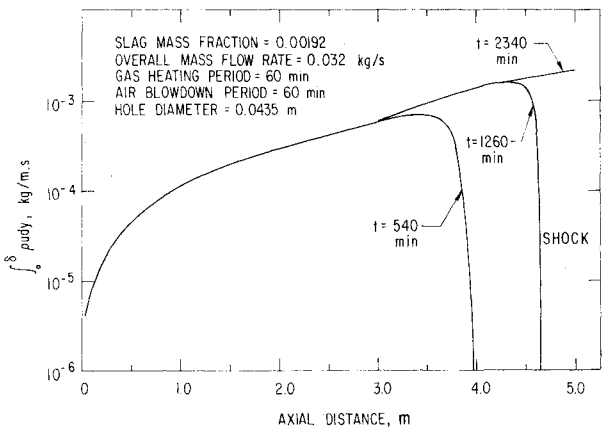

Fig. 6 Slag flow rate in liquid layer for mass flow rate of 0.032 kg/s.

about 1200 min, clogging of the passages probably will seriously impair operation of the heat exchanger.

Profile of the accumulation shock is much less acute than that shown in Fig. 3. With the increased rate of heat transfer in Fig. 4, a portion of the layer near the gas phase is at a higher temperature than the corresponding portion in Fig. 3. This permits the continuous flow of a small amount of the slag over the shock.

It is interesting to note that the continuous slag accumulation ($t \simeq 2300$ min) finally causes the complete overflow of the slag to the down side of the shock (see Fig. 4). This can be seen more clearly from Figs. 5 and 6 where the slag flow rates across the layer, as functions of x, corresponding to the profiles of Figs. 3 and 4, respectively, are shown. For the lower gas flow rate, Fig. 5 shows that no slag flow takes place across the shock. The layer profile aft of the shock is determined by the local deposition rates. The shock profile is acute. For the higher gas flow rate, on the other hand, a small amount of the slag flows over the shock, keeping its profile much less acute. At certain time, however, a precipitous deluge occurs across the shock into the downstream as seen in Fig. 6. In any case, with the large portion of the passage cross sections clogged, continuous operation of the heat exchanger is stymied once a shock is established.

V. Concluding Remarks

Transient behavior of liquid layer on a vertical surface is first analyzed near its freezing temperature. Variation of the liquid viscosity with respect to temperature and the rate of condensation are found to be the predominant parameters affecting the behavior. The governing equations comprise a wave equation. Increasing liquid viscosity in the x direction near the freezing temperature causes coalescence of the characteristics of the equation, signifying the formation of an accumulation shock. Detailed discussion of the wave phenomena leading to shock emergence is given in Sec. II.

Next, transport of the particulate matters of 1-60 μm in size in turbulent gas streams is analyzed. Expressions are developed which give the deposition rates of the particulate matters in turbulent pipe flows. These are found in Sec. III.

Analyses of Secs. II and III are combined in Sec. IV to study the accumulation of slag in a typical regenerative heat exchanger using the coal combustion product as the heat source. The numerical solutions show the shock formation predicted in Sec. II. The shock leads to clogging of the heat exchanger passages and impediment of continued operation of the exchanger. Detailed discussion is given in the preceding section.

The interface shear stress τ_s was neglected in the qualitative discussion of the liquid layer behavior in Sec. II. The numerical results of Sec. IV with τ_s shows that the general behavior is unaltered by τ_s. The shear stress simply superimposes itself on the gravity in determining the liquid flow rate and affects the position and time of the shock formation.

Acknowledgment

This work was supported by the MHD Division of the U.S. Dept. of Energy.

References

[1] Petrick, M. and Shumyatsky, B. Ya., *Open Cycle Magnetohydrodynamic Electrical Power Generation*, Argonne National Laboratory, Argonne, Ill., 1978, Chap. 9.

[2] Heywood, J. B. and Womack, G. J., *Open Cycle M.H.D. Power Generation*, Pergamon Press, New York, 1969, Chap. 2.

[3] Way, S., *Combustion Technology*, edited by H. B. Palmer and J. M. Beer, Academic Press, New York, 1974, pp. 291-319.

[4] Goodman, T. and Shea, J. J., "The Melting of Finite Slabs," *Transactions of ASME*, Vol. 7, March 1960, pp. 16-24.

[5] Scala, S. M. and Sutton, G. W., "The Two-Phase Hypersonic Laminar Boundary Layer," *Proceedings of the 1958 Heat Transfer and Fluid Mechanics Institute*, 1958, pp. 231-240.

[6] Kreith, F., *Principles of Heat Transfer*, 2nd Ed., International Textbook Co., Scranton, Penn., 1967, pp. 373-376.

[7] Chapman, A. J., *Heat Transfer*, 3rd Ed., Macmillan Publishing Co., New York, 1974, Chap. 8.

[8] Im, K. H., Chung, P. M., and Carlson, L., "Slag and Seed Deposition on Heat Exchanger Surfaces from Gas-Droplet Mixture," *17th Symposium on Engineering Aspects of Magnetohydrodynamics*, March 1978, pp. I.5.1-I.5.8.

[9] Sande, C. K., Townes, H. W., and Reiman, T. C., "Particulate Deposition in Direct Fired MHD Air Preheater," Paper 77-HT-65, *AIChE-ASME Heat Transfer Conference*, Aug. 1977.

[10] White, L. R., private communication, FluiDyne Engineering Co., Minneapolis, Minn., June 1978.

[11] Hinze, J. O., *Turbulence*, McGraw-Hill Book Co., Inc., New York, 1959, pp. 352-361.

[12] Davis, C. N., "Deposition of Aerosols from Turbulent Flow through Pipes," *Proceedings of Royal Society A289*, 1966, pp. 235-246.

[13] Capps, W., "Some Properties of Coal Slags of Importance to MHD," *16th Symposium on Engineering Aspects of Magnetohydrodynamics*, 1977, pp. VIII. 3.21-VIII. 3.25.

[14] Rodgers, M. E. and Kruger, C. H., "Fluid Mechanics and Thermal Behavior of MHD Channel Slag Layers," *17th Symposium on Engineering Aspects of Magnetohydrodynamics*, 1978, pp. C.2.1-C.2.6.